TBX20 regulates epithelial-mesenchymal transition, maintains tumor stemness and immune factor expression, and promotes immune escape in lung cancer

CHUNCAI XU[1,2], PENG ZHOU[1], YANTING ZHANG[1], LILI LI[1] and GUOWEN WANG[1]

[1]National Key Laboratory of Draggability Evaluation and Systematic Translational Medicine, Tianjin's Clinical Research Center for Cancer, Department of Bone and Soft Tissue Tumors, Tianjin Medical University Cancer Institute and Hospital, National Clinical Research Center for Cancer, Tianjin 300060, P.R. China; [2]Department of Orthopedics, Fujian Provincial Hospital, Shengli Clinical Medical College of Fujian Medical University, Fuzhou University Affiliated Provincial Hospital, Fuzhou, Fujian 350001, P.R. China

Received November 24, 2025; Accepted March 6, 2026

DOI: 10.3892/ol.2026.15562

Abstract. T-box transcription factor 20 (TBX20) serves a crucial regulatory role in the process of tumor occurrence. In lung cancer, the upregulation of TBX20 expression is positively associated with a poor prognosis; however, the specific underlying mechanism remains unclear. Therefore, in the present study, the expression of TBX20 in normal lung epithelial BEAS-2B and cancer cells A549 was detected by quantitative PCR and western blot. Lung cancer cell lines with overexpression and interference of TBX20 were constructed. Cell proliferation was detected by Cell Counting Kit-8, cell migration and invasion were detected by Transwell, and cell spheroid formation was assessed. The expression of EMT markers (E-cadherin, N-cadherin, vimentin), stemness markers (CD44, Sox2, Nanog), and immune factors (PD-L1, IL-6, CCL2) was detected by qPCR and WB. A subcutaneous lung cancer model in nude mice was established. After 4 weeks, the tumor volume was observed. The expression of E-cadherin, N-cadherin, vimentin, CD44, and PD-L1 in tumor tissues was detected by IHC. The infiltration of immune cells (CD8+T, CD4+T, M1/M2 macrophages) was detected by flow cytometry. *In vitro* experiments revealed that the expression levels of TBX20 were increased in the A549 lung cancer cells compared with those in BEAS-2B normal lung epithelial cells. In addition, cell viability, migration, invasion and spheroid formation capacity were greater in the A549 group than in the BEAS-2B group. Compared with in the negative control (NC) group, the TBX20 overexpression plasmid (oe-TBX20) group exhibited enhanced cell viability, migration, invasion and spheroid formation capacity. Furthermore, E-cadherin expression was reduced, whereas N-cadherin, vimentin, Sox2, CD44, Nanog, PD-L1, IL-6 and CCL2 expression levels were elevated. Notably, these changes were reversed in the TBX20 knockdown group. *In vivo* experiments revealed that compared with in the NC group, the oe-TBX20 group had significantly increased tumor volume, decreased E-cadherin levels, and elevated expression levels of TBX20, N-cadherin, vimentin, CD44 and PD-L1. Compared with NC group, the oe-TBX20 group exhibited significantly lower infiltration of $CD4^+$ T and $CD8^+$ T cells and M1-type macrophage, whereas that of M2-type macrophages and regulatory T cells increased. Conversely, these indicators were reversed in the short hairpin RNA-TBX20 group. In conclusion, TBX20 may induce epithelial-mesenchymal transition and stem cell characteristics, enhance the malignant behavior of lung cancer cells, and upregulate PD-L1 expression to promote immune escape.

Correspondence to: Dr Guowen Wang, National Key Laboratory of Draggability Evaluation and Systematic Translational Medicine, Tianjin's Clinical Research Center for Cancer, Department of Bone and Soft Tissue Tumors, Tianjin Medical University Cancer Institute and Hospital, National Clinical Research Center for Cancer, 1 Huanhu Road West, Tiyuan North, Hexi, Tianjin 300060, P.R. China
E-mail: wangguowen@tmu.edu.cn

Key words: lung cancer, T-box transcription factor 20, epithelial-mesenchymal transition, tumor stemness, immune factors, immune escape

Introduction

According to data from 2024, lung cancer remains the most commonly diagnosed type of cancer worldwide (1). Despite recent advancements in surgical techniques, and the application of targeted therapies and immunotherapies, the overall survival rate for patients with lung cancer remains low, with the age-standardized 5-year overall survival rate estimated at 10-20% (2). Notably, immune escape, metastasis and recurrence are factors that collectively represent major therapeutic hurdles for patients with lung cancer (3). Therefore, identifying key driver genes of immune evasion that can be targeted, elucidating their oncogenic mechanisms and developing targeted combination strategies are urgently needed to overcome therapeutic bottlenecks and prolong patient survival.

The biological characteristics of lung cancer; for example, proliferation, anti-apoptosis, invasion, metastasis, drug

resistance and immune evasion, are essentially the result of dysregulated gene expression programs, with transcription factors (TFs) serving as the primary switches for these programs (4). T-box TFs (TBXs), a family of proteins containing T-box DNA-binding domains, are widely distributed across the animal kingdom. TBXs serve crucial roles in embryonic development, cellular differentiation, organ formation, and various physiological and pathological processes. Numerous studies have demonstrated their pivotal roles in regulating epithelial-mesenchymal transition (EMT), maintaining tumor stem cell properties, inducing apoptosis, promoting tumor cell proliferation and enhancing tumor drug resistance (5-9). Growing evidence has indicated that the T-box family serves as a promising biomarker, with pivotal roles in cancer diagnosis, identification of therapeutic targets and prognosis (10). As a key member of the T-box family, TBX20 has garnered attention because of its roles in various physiological and pathological processes. In cardiomyocytes, TBX20 has been shown to activate the bone morphogenetic protein 2 (BMP2)/phosphorylated (p)-Smad1/5/8 and PI3K/AKT/GSK3β/β-catenin signaling pathways, promoting cell proliferation and survival (11). In colorectal cancer, TBX20 directly binds to Ku70/Ku80 through its intermediate domain, blocking the formation of heterodimers between the two proteins. This inhibits non-homologous end joining-mediated double-strand break repair, leading to cumulative DNA damage and genomic instability, thereby suppressing cell proliferation and enhancing sensitivity to radiotherapy/daunorubicin (12). TBX20 is clearly not merely a developmental regulator but also a key TF with the potential to modulate cancer progression. Notably, the role of TBX20 in heart and lung development has been extensively studied (13,14), but the specific mechanism of TBX20 in lung cancer remains unclear. To elucidate the tumorigenic role of TBX20 in lung cancer, *in vitro* and *in vivo* experiments were performed to elucidate how TBX20 promotes cell proliferation and immune evasion. The value of TBX20 as a prognostic marker and therapeutic target was also evaluated.

Materials and methods

Cell culture and transfection. The human normal lung epithelial cell line BEAS-2B, and the human non-small cell lung cancer cell lines A549 and HCI-H1975 used in this study were all purchased from The Cell Bank of Type Culture Collection of The Chinese Academy of Sciences. The cells were cultured in DMEM (Wuhan Servicebio Technology Co., Ltd.) supplemented with 10% fetal bovine serum (FBS; Nanjing BioChannel Biotechnology Co., Ltd.) and 1% penicillin-streptomycin (Wuhan Servicebio Technology Co., Ltd.), at 5% CO_2 and 37˚C. Small interfering (si)RNA-TBX20 (si-TBX20) and siRNA-negative control (NC) were transfected into A549 cells using Lipofectamine® 3000 transfection reagent (Invitrogen; Thermo Fisher Scientific, Inc.). TBX20 overexpression plasmid (oe-TBX20) was also transfected into A549 cells using pRP[Exp]-EGFP/Puro-CAG>hTBX20 [Yunzhou Biosciences (Guangzhou) Co., Ltd.); at the same time, the empty vector pRP[Exp]-EGFP/Puro-CAG (without the TBX20 insertion fragment) was used as the negative control. A549 cells were added to six-well plates, with $2x10^6$ cells per well, and 2 μl DMEM medium was added. A total of 5 μg of DNA or siRNA, was added at 25˚C for 6 h. Culture medium was removed, and 10% serum-containing DMEM medium was added, and the cells were further cultured at 37˚C for 24 h. Finally, the transfection efficiency was observed under a fluorescence microscope. The sequences of siRNA-TBX20, siRNA-NC and oe-TBX20 were designed and synthesized by Sangon Biotech (Shanghai) Co., Ltd. The siRNA sequences used are as follows: siRNA-TBX20, forward 5'-CCGAGA UGAUCAUCACCAAGU-3', reverse 5'-UUGGUGAUGAUC AUCUCGGUG-3'; siRNA-NC, forward 5'-UUCUCCGAA CGUGUCACGUUU-3' and reverse 5'-ACGUGACACGUU CGGAGAAUU-3'.

Western blotting. Total cellular protein was extracted from A549 and HCI-H1975 using a protein extraction kit (cat. no. BC3710; Beijing Solarbio Science & Technology Co., Ltd.) according to the manufacturer's protocol. After determining the protein concentration using BCA Protein Quantification kit, loading buffer was added and the samples were incubated at 95˚C for denaturation. SDS-PAGE was performed on 12% gels with 30 μg protein/lane. Proteins were transferred to a PVDF membrane, which was blocked with 5% skim milk solution for 2 h at 25˚C. The PVDF membrane was incubated with diluted primary antibodies at 4˚C for 12 h, washed and incubated with diluted secondary antibodies on ice in the dark for 2 h. An ECL reagent (cat. no. MA0186; Dalian Meilun Biology Technology Co., Ltd.) was used for visualization and a gel imaging system (SH-523; Hangzhou Shenhua Technology Co., Ltd.) was used for development. ImageJ (National Institutes of Health, V1.8.0.112) was used to calculate the gray values of proteins. The following antibodies were used in the present study: TBX20 (cat. no. 83414-5-RR; 1:1,000; Wuhan Sanying Biotechnology), E-cadherin (cat. no. 60335-1-Ig; 1:1,000; Wuhan Sanying Biotechnology), N-cadherin (cat. no. 66219-1-Ig; 1:2,000; Wuhan Sanying Biotechnology), vimentin (cat. no. A19607; 1:1,000; ABclonal Biotech Co., Ltd.), CD44 (cat. no. 84854-5-RR; 1:500; Wuhan Sanying Biotechnology), Sox2 (cat. no. 66411-1-Ig; 1:500; Wuhan Sanying Biotechnology), Nanog (cat. no. 14295-1-AP; 1:500; Wuhan Sanying Biotechnology), PD-L1 (cat. no. 66248-1-Ig; 1:100; Wuhan Sanying Biotechnology), IL-6 (cat. no. A0286; 1:200; ABclonal Biotech Co., Ltd.), CCL2 (cat. no. MA5-17040; 1:500; Thermo Fisher Scientific, Inc.) and β-actin (cat. no. 81115-1-RR; 1:2,000; Wuhan Sanying Biotechnology) primary antibodies, and HRP-conjugated rabbit anti-mouse and goat anti-rabbit secondary antibodies (cat. nos. ab6728 and ab6721; 1:5,000; Abcam).

Reverse transcription-quantitative PCR (RT-qPCR). Total RNA was extracted from A549 and HCI-H1975 cells using a TRIzol kit (Invitrogen), and the RNA concentration and purity were measured with a NanoDrop microplate spectrophotometer (Thermo Fisher Scientific, Inc.). cDNA was subsequently synthesized by RT using a PrimeScript RT-PCR kit (Takara Bio, Inc.), performed according to manufacturer's protocol. Finally, qPCR was performed on cDNA using the eQ9600 real-time fluorescent qPCR detection system (Suzhou Dongsheng Xingye Scientific Instruments Co., Ltd.), Thermocycling conditions were as follows: Pre-denaturation at 95˚C for 3 min; Denaturation at 95˚C for 5 sec, annealing

Table I. Primer sequences.

Gene	Primer sequence, 5'-3'
β-actin	F: GATTCCTATGTGGGCGACGA
	R: AGGTCTCAAACATGATCTGGGT
TBX20	F: CAACCCCAAATCGAGGGTCA
	R: CCGATGGTGTCAGAGGCATT
N-cadherin	F: CCTGCTTTCATTCTGACATACCT
	R: GCTTCTCACGGCATACACCA
E-cadherin	F: TGGTACCTGGCAAGATGCAG
	R: GGGGGCTTCATTCACATCCA
Vimentin	F: CAGATGCGTGAAATGGAAGAGA
	R: GTGATGCTGAGAAGTTTCGCTG
CD44	F: ACTGGAACCCAGAAGCACAC
	R: TGTCCCTGTTGTCGAATGGG
Sox2	F: ATGGACAGTTACGCGCACAT
	R: CGAGCTGGTCATGGAGTTGT
Nanog	F: AGATGTCTTCTGCTGAGATGC
	R: TTGCGTCACACCATTGCTA
PD-L1	F: TGCCGACTACAAGCGAATTACTG
	R: CTGCTTGTCCAGATGACTTCGG
IL-6	F: AGTGAGGAACAAGCCAGAGC
	R: AGCTGCGCAGAATGAGATGA
CCL2	F: TCTCGCCTCCAGCATGAAAG
	R: GGCATTGATTGCATCTGGCT

F, forward; R, reverse; TBX20, T-box transcription factor 20.

at 60˚C for 30 sec, extension at 72˚C for 20 sec, a total of 40 cycles. The mRNA expression levels of TBX20, vimentin, N-cadherin, E-cadherin, CD44, Sox2, Nanog, PD-L1, IL-6 and CCL2 were analyzed using the $2^{-\Delta\Delta Cq}$ method (15), with β-actin as the internal reference gene. The primer sequences are shown in Table I.

Cell Counting Kit (CCK)-8. After 48 h of transfection, A549 cells from each group were seeded at 2,000 cells/well in a 96-well plate. After 24 h of incubation, 20 μl CCK-8 reagent (GlpBio, GK10001) was added per well, followed by a 2-h, 37˚C incubation. The absorbance was measured at 450 nm using a microplate reader to assess cell viability, as follows: Cell viability (%)=($OD_{experimental\ group}$/$OD_{positive\ drug\ group}$/$OD_{control\ group}$) x100.

Transwell migration and invasion assays. After the A549 and HCI-H1975 cells were resuspended in serum-free DMEM, 1x10^4 cells were inoculated into each well of a 24-well low-adhesion plate and total volume is 500 μl. A 200-μl cell suspension was added to the upper chamber of the Transwell system. The lower chamber was supplemented with 500 μl DMEM containing 20% fetal bovine serum. After incubation at 37˚C for 24 h, the supernatant and cell debris were removed. At 25˚C, the cells were fixed with 100% methanol for 30 min, stained with 0.1% crystal violet for 20 min and washed with PBS. Finally, three randomly selected fields were observed under a x200 inverted light microscope to assess cell migration. For the invasion assay, the same protocol was performed; however, the upper chamber of the Transwell system was coated with 8% Matrigel at 37˚C for 3 h before cell seeding.

Spheroid formation assay. A549 cells were seeded at $1x10^4$ cells/500 μl volume per well into low-adhesion 24-well plates. DMEM/F12 (Wuhan Servicebio Technology Co., Ltd, containing 20 ng/ml epidermal growth factor, 10 ng/ml basic fibroblast growth factor and 10 μg/ml B27) was added and the cells were incubated at 37˚C for 24, 48 and 72 h. Images were captured using an light microscope at 72 h post-seeding, after which the spheroids were counted.

Nude mouse transplantation tumor model. A total of 12 male BALB/c nude mice (age, 5-6 weeks; body weight, ~16 g) were provided by Hunan Sileke Jingda Experimental Animal Co., Ltd. [license no. SCXK (Xiang) 2025-0004] and the experiment was approved by the Animal Ethics Committee of Fuzhou University Affiliated Provincial Hospital [approval no. IACUC-FPH-SL-20250527[1092]). Human peripheral blood mononuclear cells (PBMCs) were purchased from the American Type Culture Collection (cat. no. PCS-800-011). The use of commercially available anonymous primary cells was exempted for ethics review by the Ethics Committee of Fuzhou University Affiliated Provincial Hospital. The mice were randomly divided into four groups: A549, A549 + sh-NC, A549 + short hairpin (sh)RNA-TBX20 (sh-TBX20; A549 cell line stably transduced with sh-TBX20 lentiviral plasmid) and A549 + oe-TBX20 (A549 cell line stably transfected with pcDNA3.1-oe-TBX20). Each group contained 3 mice.

Using pcDNA3.1 as the vector, restriction endonucleases *Nhe*I and XbaI were used as the cutting sites. Mutant primers were designed and synthesized by Shanghai Sangon Biotech Co., Ltd., and the target gene was amplified by PCR to obtain the mutant TBX20 cDNA sequence. The forward primer sequence was 5'-GCTAGCATGGCGGCGGCGGCGGCG GCGGC-3' (containing *Nhe*I site) and the reverse primer sequence was 5'-TCTAGATCAGTCATCATCATCGTCATC AT-3' (containing XbaI sit). For the T262M point mutation, the mutagenic primer sequences were as follows: Forward 5'-GCT AGCATGGCGGCGGCGGCGGCGGC-3' and reverse 5'-TCTAGATCAGTCATCATCATCGTCATCAT-3', with the mutation introduced by site-directed mutagenesis using PrimeSTAR high-fidelity DNA polymerase (Takara Bio, Inc.; cat. no. R045A). PCR amplification was performed with the following conditions: Initial denaturation at 98˚C for 2 min; 35 cycles of 98˚C for 10 sec, 60˚C for 15 sec, and 72˚C for 2 min; final extension at 72˚C for 5 min. The target gene was recombined and transformed with pcDNA3.1, and the obtained sequence was confirmed by Sanger sequencing (Shanghai Sangon Biotech Co., Ltd.) to ensure its accuracy. Wild-type TBX20-pcDNA3.1 and mutant TBX20-T262M-pcDNA3.1 overexpression plasmids were constructed by Shanghai Sangon Biotech Co., Ltd.

The second-generation lentiviral packaging system was used for lentivirus production. 293T cells (human embryonic kidney cells; American Type Culture Collection, Cat. No. CRL-3216) were seeded at $4x10^6$ cells per 10-cm dish 24 h prior to transfection. At 70-80% confluence, cells were co-transfected with 7.5 μg shRNA-TBX20 plasmid

(forward, 5'-CCGGGCAGAAGATCAAGATCAATTCTC GAGAATTGATCTTGATCTTCTGCTTTTTG-3' and reverse, 5'-AATTCAAAAAGCAGAAGATCAAGATCA ATTCTCGAGAATTGATCTTGATCTTCTGC-3'), plasmid backbone (pL KO.1-puro Lentiviral shRNA expression vector (purinomycin resistance); Sigma-Aldrich, Cat. No. SHC001), 5.6 μg psPAX2 packaging plasmid (Addgene, 12260), and 1.9 μg of pMD2.G envelope plasmid (Addgene, Inc.; cat. no. 12259) using Lipofectamine 3000 (Thermo Fisher Scientific, Inc., L3000015) according to the manufacturer's instructions. The plasmid ratio was 4:3:1 (shRNA:psPAX2:pMD2.G). Transfection was performed in Opti-MEM reduced serum medium at 37˚C, 5% CO_2 for 12 h, after which the medium was replaced with fresh DMEM containing 10% FBS. At 48 and 72 h after transfection, supernatants and centrifuge at 500 x g for 5 min at 4˚C. Then filter through a 0.45 μm PVDF membrane. After aliquoting, store at -80˚C. Viral titer was determined by RT-qPCR.

For lentiviral transduction, A549 cells were seeded at $2x10^5$ cells per well in 6-well plates. When cell density reached 50% confluence, lentivirus at MOI of 8 were added. The cells were gently mixed and cultured at 37˚C for 24 h. Cells were selected using puromycin (2 μg/ml). Continuous screening was conducted for 5 days. Cells were cultured for 24 h before subsequent experiments. Infection efficiency of the lentivirus was verified by RT-qPCR and Western blot. Culture medium containing puromycin (1 μg/ml) was used to maintain the cells.

Stable overexpression and interference cell lines (oe-TBX20 and shTBX20) of the TBX20 gene were constructed. A549 cells that stably expressed oe-TBX20 and shTBX20 were resuspended in PBS ($2x10^7$ cells/ml) and gently mixed with an equal volume of Matrigel to obtain a cell-scaffold mixture with a final concentration of $1.0x10^7$ cells/ml. Subsequently, 100 μl mixture was injected subcutaneously into the right axilla of each nude mouse. PBMCs were expanded by culturing in a complete medium containing 100 ng/ml IL-2. The cells were resuspended in sterile PBS to a concentration of $1.0x10^8$ cells/ml and stored on ice for later use. The PBMCs were resuspended in PBS at a concentration of $1.0x10^8$ cells/ml, and 100 μl PBMC suspension was injected subcutaneously at the edge of the tumor nodule (not directly injected into the tumor center). At 30 days after the injection of tumor cells, the mice were euthanized by intraperitoneal injection with 1% pentobarbital sodium (200 mg/kg) and decapitation, and the tumors were removed and weighed. Humane endpoints were as follows: Maximum tumor diameter exceeded 20 mm; maximum tumor volume exceeded 2,000 mm^3; obvious signs of cachexia. No mice were sacrificed prematurely.

Immunohistochemistry (IHC). Tumor tissues were fixed with 4% paraformaldehyde solution for 24 h at 4˚C. The tissue blocks were sectioned into 4 μm slices, baked at 60˚C for 30 min. The sections underwent routine xylene dewaxing, followed by alcohol hydration with a gradient, and three washes with distilled water for 3 min each. Subsequently, they were rinsed three times with PBS for 3 min each. The antigen retrieval solution containing EDTA, pH 9.0, Wuhan Servicebio Technology Co., Ltd.) was boiled in a high-pressure cooker for 2 min. The sections were then placed in an incubation chamber, and 3% hydrogen peroxide solution was added. After incubation at 25˚C for 12 min, the sections were rinsed three times with PBS solution for 3 min each. Then, 5% goat serum (Nanjing SenBeiJia Biological Technology Co., Ltd.) was added, and the sections were incubated at 25˚C for 20 min. TBX20 primary antibody (Thermo Fisher Scientific, Inc., cat. no. PA5-110464; 1:500) was added overnight at 4˚C. Sections were rinsed three times with PBS buffer for 2 min each to remove excess primary antibody. The secondary antibody (HRP-labeled rabbit anti-IgG, 1:500; cat. no. TBAG0030, Wuhan Servicebio Technology Co., Ltd.) was added, and the sections were incubated at 25˚C for 30 min. After rinsing three times with PBS buffer for 2 min each, the prepared DAB chromogenic solution (Wuhan Servicebio Technology Co., Ltd.) was added. The staining was observed under an light microscope. Sections were stained with hematoxylin (Beijing Biosharp Technology Co., Ltd) for 5 min, followed by rinsing with distilled water. Staining was evaluated independently by two pathologists who were blinded to the clinical data. Positive staining was defined as brown nuclear staining. Images of five representative high-power fields (magnification, x400) per tumor were photographed. The percentage of positive tumor cells was recorded.

Flow cytometry. Flow cytometry was used to detect immune cells. Fresh tumor tissues were placed in cold PBS and minced with ophthalmic scissors. The tissue was then transferred to a 15-ml centrifuge tube and digested with 5 ml digestion buffer (RPMI-1640 + 2 mg/ml collagenase IV + 20 μg/ml DNase I) in a 37˚C water bath with oscillation. After the digestion was complete, 5 ml RPMI-1640 containing 10% FBS was added to terminate the reaction. The suspension was filtered through a 70-μm cell sieve to collect the single-cell suspension and was then centrifuged at 400 x g for 5 min at 4˚C, after which the supernatant was discarded, and the cells were resuspended in PBS. Next, 1 ml ACK lysis buffer was added, the mixture was incubated for 2 min and the reaction was terminated with PBS. The cell suspension was adjusted to $1x10^6$ cells/100 μl, and was transferred to a flow cytometry tube. Fc blocking agent (Rat Anti-Mouse CD16/CD32, BD Biosciences, cat. No. 553142) was added, and the sample was incubated at 4˚C for 10 min. A surface antibody mixture (CD3, CD4, CD8, Foxp3, CD86 and CD206) was then added and incubated at 4˚C in the dark for 30 min. The labelled antibodies for CD4+ T cells are: CD3 (FITC anti-human CD3, BioLegend, Inc., cat. No. 317306), CD4 (PE-anti-human CD4, BioLegend, Inc., Cat. No. 300508). The labelled antibodies for CD8+ T cells are: CD3, CD8 (PE anti-human CD8 Antibody, BioLegend, Inc., Cat. No. 344705). The labelled antibodies for Treg cells are: CD3, CD4, Foxp3 (APC Anti-FOXP3Antibody[3G3], Abcam, Cat. No. ab200568). The labelled antibody for M1 cells is: CD86 (FITC anti-human CD86 Antibody, BioLegend, Inc., Cat. No. 374203). The labelled antibody for M1 cells is: CD206 (FITC anti-human CD206 (MMR) Antibody, BioLegend, Inc., Cat. No. 321103). The suspension was subsequently washed twice with PBS (4˚C, 300 x g, 5 min each), the supernatant was discarded, and a FoxP3 fixation/permeabilization kit (eBioscience™ Foxp3/Transcription Factor Staining Buffer Set; Cat. no. 00-5523-00, Thermo Fisher Scientific, Inc.) was used. Briefly, 100 μl fixation/membrane disruption solution was added and the sample was incubated at 25˚C in the dark for 30-60 min. The sample was then washed once with 1X

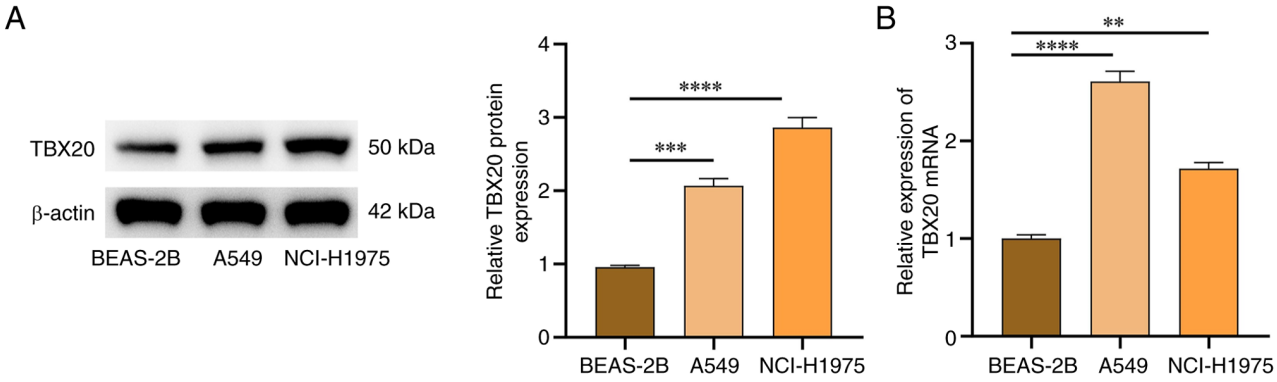

Figure 1. Western blotting and RT-qPCR analyses of TBX20 expression in lung cancer cells. (A) Western blot analysis of TBX20 protein expression. (B) RT-qPCR analysis of TBX20 mRNA expression. Data are presented as the mean ± standard deviation (n=3). **P<0.01, ***P<0.001 and ****P<0.0001. RT-qPCR, reverse transcription-quantitative PCR; TBX20, T-box transcription factor 20.

membrane disruption buffer and then centrifuged (4˚C and 400 x g for 5 min) to remove the supernatant. The sample was then resuspended in 50 μl membrane disruption buffer, PE-labelled anti-FoxP3 antibody was added and the sample was incubated at 4˚C in the dark for 30 min. The cells were then washed once with membrane disruption buffer, resuspended in 200-300 μl PBS and prepared for flow cytometry. A BD LSRFortessa flow cytometer (BD Biosciences) with appropriate laser and filter settings was used. At least 50,000 $CD45^+$ leukocyte events per sample were collected, isotype control (Mouse IgG1, κ isotype Ctrl antibody, BioLegend, Inc., Cat. no. 400105) and single-stain compensation tubes were used for normalization, and the data were analyzed using FlowJo v10 software (BD Biosciences).

Statistical analysis. Statistical analysis was performed using SPSS26.0 (IBM Corp.) and GraphPad Prism 8.0.2 (Dotmatics), with all experiments repeated three times. Quantitative data (conforming to normality and variance homogeneity) are presented as the mean ± standard deviation. One-way ANOVA was used for inter-group comparisons, after which, the SNK post hoc test was used to analyze datasets containing ≤3 groups, whereas multiple comparisons between >3 groups were analyzed using the Tukey post hoc test. Independent samples t-test was employed for comparisons between two groups. P<0.05 was considered to indicate a statistically significant difference.

Results

TBX20 expression in cancer cells. The expression levels of TBX20 in lung cancer cells were assessed by western blotting, which revealed that TBX20 protein expression was significantly higher in in A549 and NCI-H1975 cancer cells compared with that in BEAS-2B cells (P<0.05; Fig. 1A). qPCR further confirmed the statistically significant increases in TBX20 mRNA expression levels in these cell lines (P<0.05; Fig. 1B). As the expression of TBX20 mRNA was highest in A549, A549 cells were used for subsequent experiments.

Effects of TBX20 on lung cancer cell viability, migration, invasion and spheroid formation. The effects of TBX20 overexpression/silencing were subsequently investigated in lung cancer cells. The successful transfection of si-TBX20 and oe-TBX20 is shown in Fig. 2A and B. Compared with the BEAS-2B group, the A549 group exhibited significantly greater cell viability (Fig. 2C), migration (Fig. 2D and G), invasion (Fig. 2E and G) and spheroid formation capacity (Fig. 2F and G) (P<0.05), whereas no significant differences were observed between the A549 and A549-siNC groups (P>0.05). Following TBX20 overexpression, compared with in the A549-NC group, cell viability, migration and invasion, and spheroid formation capacity were significantly increased (P<0.05). By contrast, after TBX20 silencing, cell viability, migration and invasion and spheroid formation capacity were significantly reduced compared with in the A549-siNC group (P<0.05).

Effects of TBX20 on the expression levels of EMT-, stemness- and immune-associated protein and genes in lung cancer cells. To evaluate the effects of TBX20 overexpression/silencing on EMT, stemness and immune activity in lung cancer cells, western blotting and RT-qPCR were used to measure the expression levels of EMT markers (E-cadherin, N-cadherin and vimentin) (16), stemness-related markers (CD44 and Nanog) (17) and immune-related cytokines (PD-L1, IL-6 and CCL2) (18). The results of western blotting (Fig. 3A) revealed that, compared with in the BEAS-2B group, the A549 group exhibited significantly reduced E-cadherin protein expression; higher N-cadherin and vimentin levels; higher CD44 and Nanog expression; and higher expression levels of PD-L1, IL-6 and CCL2 (P<0.05; Fig. 3B-D and F-J). Compared with the A549 + NC group, the expression of Sox2 in the A549 + oe-TBX20 group showed no significant change (Fig. 3E). However, no significant differences were observed between the A549 and A549-NC groups (P>0.05). After TBX20 overexpression, the expression levels of E-cadherin were significantly lower, whereas those of N-cadherin, vimentin, CD44, Nanog, PD-L1 and IL-6 levels were higher than those in the A549-NC group (P<0.05). Conversely, compared with in the A549-NC group, TBX20 silencing led to increased E-cadherin expression, but significantly decreased N-cadherin, vimentin, CD44, PD-L1 and IL-6 levels (P<0.05).

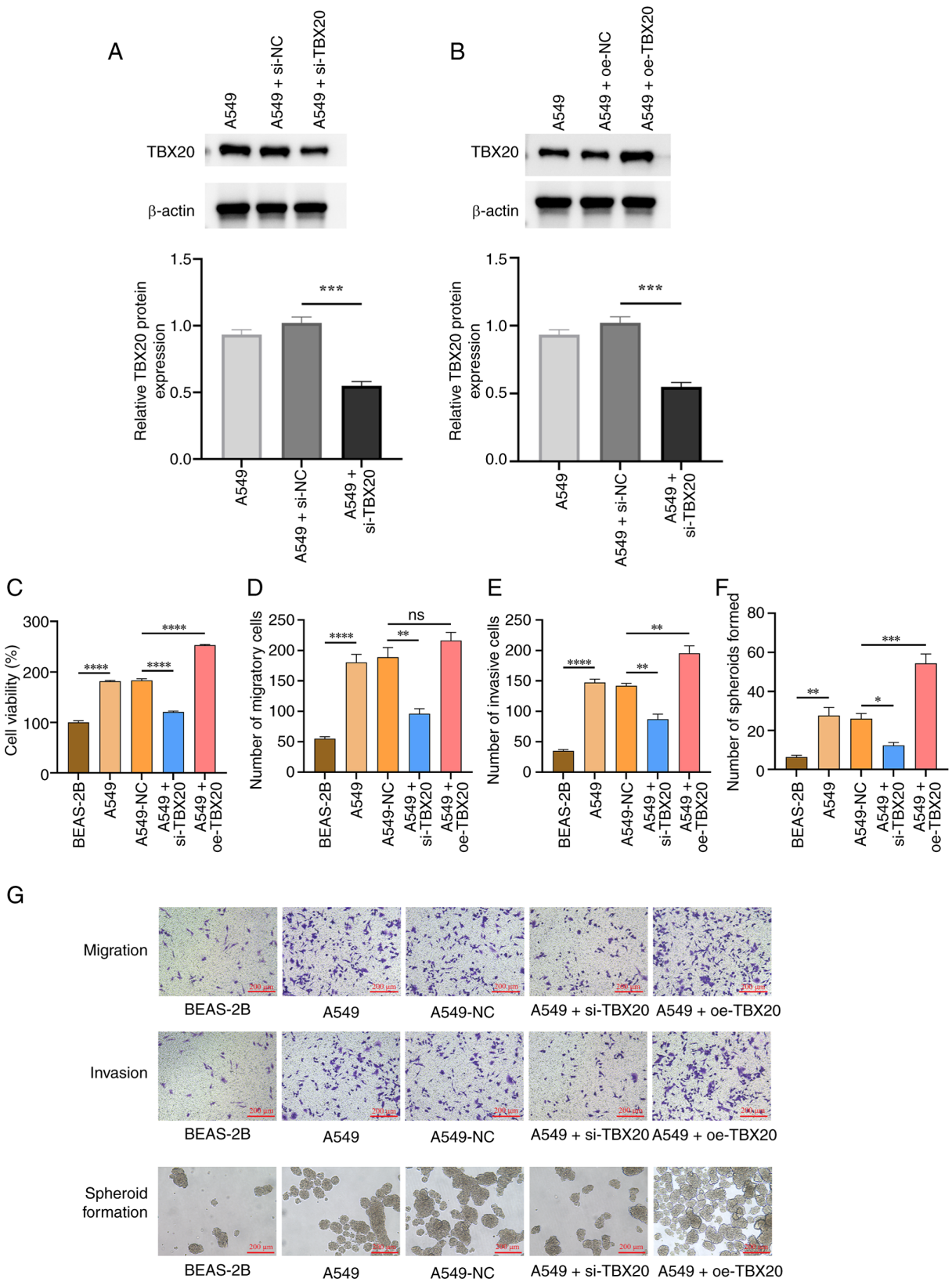

Figure 2. Effects of oe-TBX20 and si-TBX20 on lung cancer cell viability, migration, invasion and spheroid formation. (A and B) Western blotting confirmed that TBX20 transfection was successful. Protein expression levels of TBX20 in A549 cells after (A) si-TBX20 and (B) oe-TBX20 transfection. (C) Cell viability, (D) cell migration, (E) cell invasion and (F) cell spheroid formation were assessed. (G) Transwell and sphere formation assay images (magnification, x100). Data are presented as the mean ± standard deviation (n=3). *P<0.05, **P<0.01, ***P<0.001 and ****P<0.0001. NC, negative control; oe, overexpression; si, small interfering; TBX20, T-box transcription factor 20; ns, not significant (P>0.05)..

The RT-qPCR results revealed that compared with in the BEAS-2B group, the A549 group exhibited significantly lower E-cadherin mRNA expression, and significantly higher mRNA expression levels of N-cadherin, vimentin, Sox2, CD44,

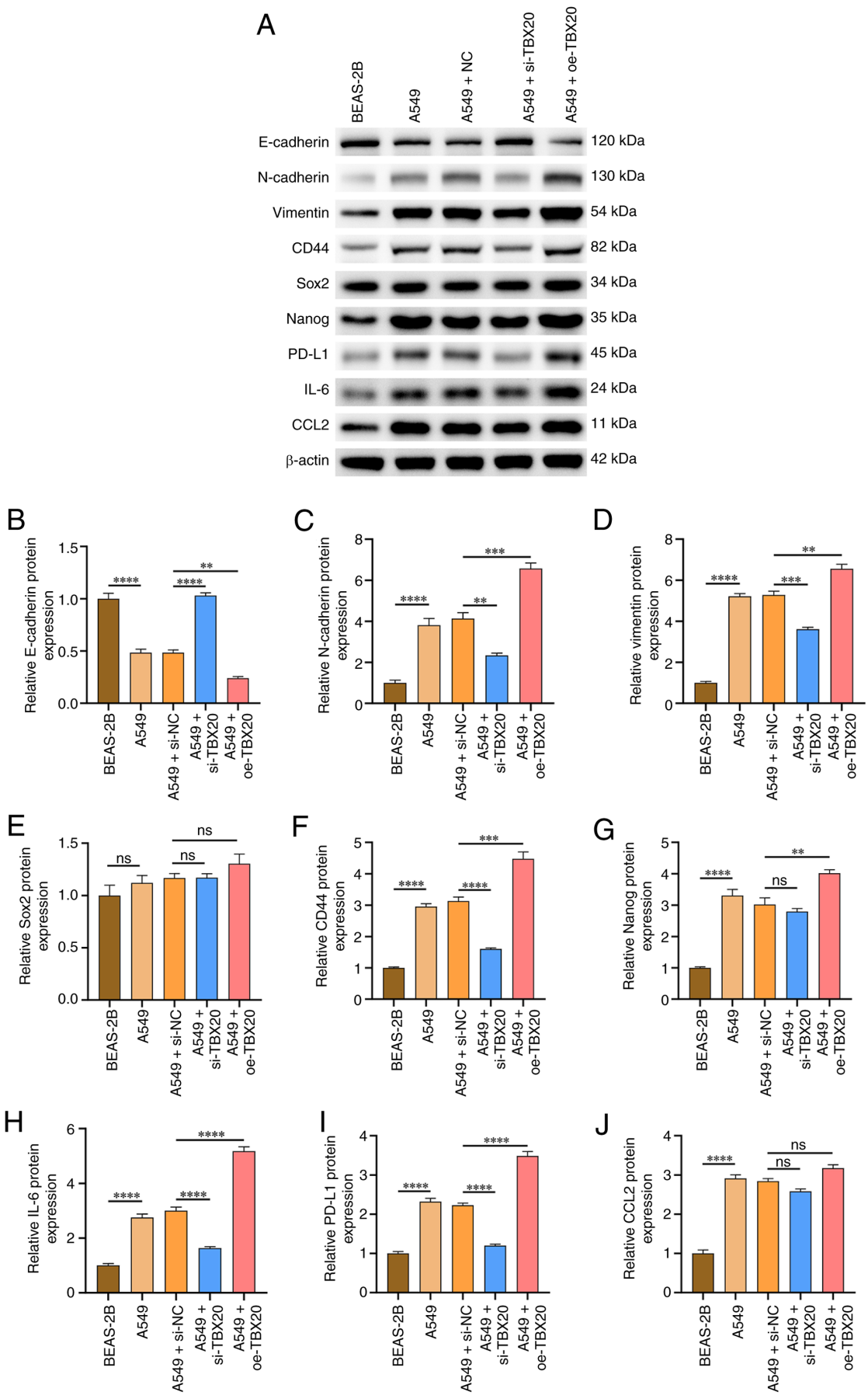

Figure 3. Effects of oe-TBX20 and si-TBX20 on epithelial-mesenchymal transition- and stemness phenotype-related proteins in lung cancer cells. (A) Western blot analysis. Protein expression levels of (B) E-cadherin, (C) N-cadherin, (D) vimentin, (E) Sox2, (F) CD44, (G) Nanog, (H) IL-6, (I) PD-L1 and (J) CCL2. Data are presented as the mean ± standard deviation (n=3). **P<0.01, ***P<0.001, ****P<0.0001 and ^{ns}P>0.05. NC, negative control; oe, overexpression; si, small interfering; TBX20, T-box transcription factor 20.

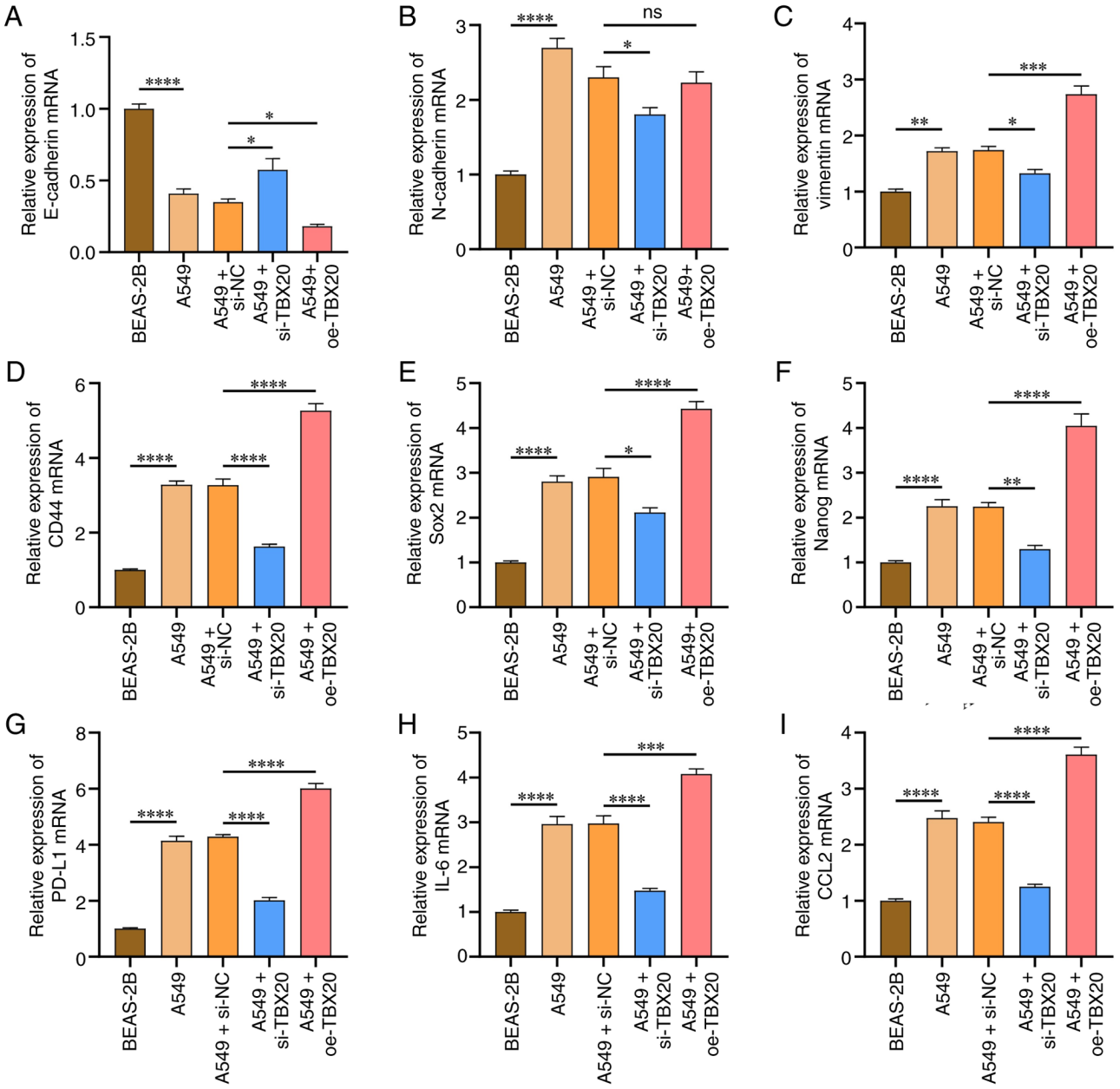

Figure 4. Effects of oe-TBX20 and si-TBX20 on epithelial-mesenchymal transition- and stemness phenotype-associated mRNA expression in lung cancer cells. mRNA expression levels of (A) E-cadherin, (B) N-cadherin, (C) vimentin, (D) CD44, (E) Sox2, (F) Nanog, (G) PD-L1, (H) IL-6 and (I) CCL2. Data are presented as the mean ± standard deviation (n=3). *P<0.05, **P<0.01, ***P<0.001, ****P<0.0001 and ^{ns}P>0.05. NC, negative control; oe, overexpression; si, small interfering; TBX20, T-box transcription factor 20.

Nanog, PD-L1, IL-6 and CCL2 (P<0.05; Fig. 4). However, no significant differences were observed between the A549 and A549-NC groups (P>0.05). After TBX20 was overexpressed, compared with the A549-NC group, E-cadherin expression was significantly decreased, whereas the levels of vimentin, Sox2, CD44, Nanog, PD-L1, IL-6 and CCL2 were significantly increased (P<0.05). Conversely, after TBX20 silencing, compared with in the A549-NC group, E-cadherin expression was significantly increased, and the levels of N-cadherin, vimentin, Sox2, CD44, Nanog, PD-L1, IL-6 and CCL2 were decreased (P<0.05).

Effects of TBX20 overexpression and silencing on subcutaneous tumor growth in nude mice. *In vivo* experiments were conducted to evaluate the effects of TBX20 overexpression and silencing on tumor size. The expression levels of TBX20 in the A549 + oe-TBX20 group were significantly greater than those in the A549 + NC group (P<0.05), whereas the A549 + sh-TBX20 group exhibited significantly lower expression (P<0.05), confirming successful transfection (Fig. 5A). At 4 weeks after subcutaneous tumor transplantation, tumor volume measurements revealed that the tumors in the A549 + oe-TBX20 group were significantly larger than those in the A549-NC group (P<0.05); the maximum diameter and tumor volume in the A549 + oe-TBX20 group were 20 mm and 1,273 mm^3, respectively, whereas those in the A549 + sh-TBX20 group were significantly smaller (P<0.05; Fig. 5B and C).

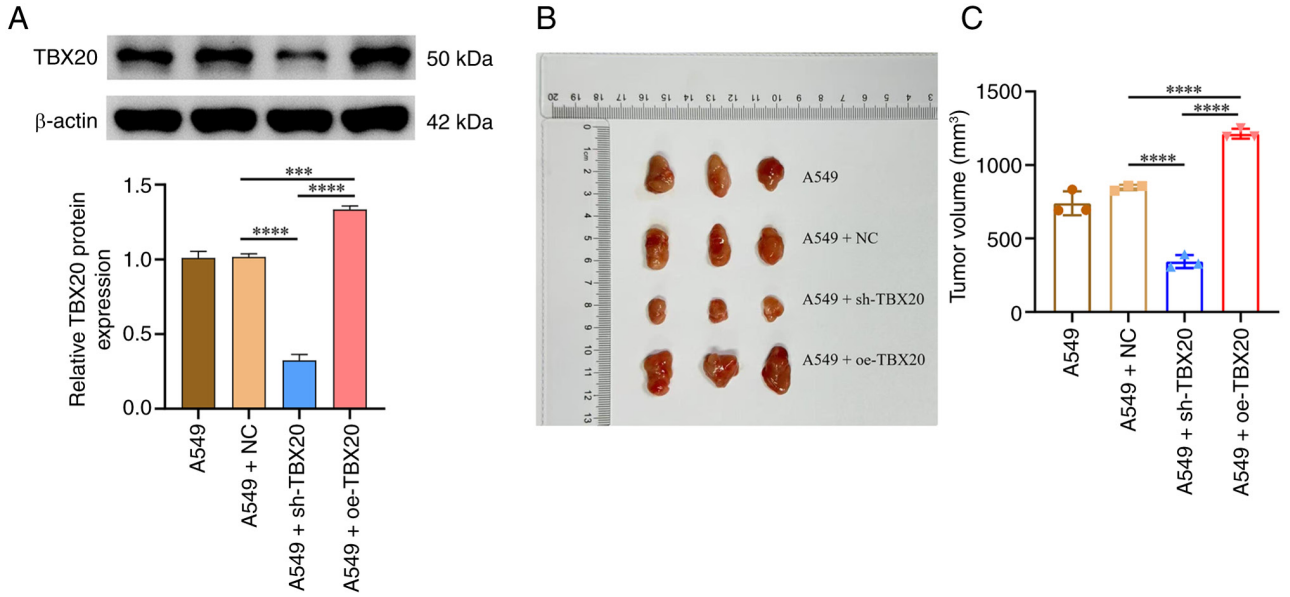

Figure 5. Tumor volume of A549 subcutaneous tumor models. (A) TBX20 expression in nude miceinjected with A549 cells. (B) Subcutaneous tumors at 4 weeks post-transplantation (three representative tissues are shown for illustration). (C) Comparison of tumor volume across the four groups. Data are presented as the mean ± standard deviation (n=3). ***P<0.001 and ****P<0.0001. NC, negative control; oe, overexpression; si, small interfering; TBX20, T-box transcription factor 20.

Effects of TBX20 overexpression and silencing on the expression of EMT and stemness markers in subcutaneous tumors from nude mice. To assess the effects of TBX20 on tumor EMT and stemness markers in nude mice, IHC was performed (Fig. 6A) to detect the expression levels of E-cadherin, N-cadherin and vimentin (EMT markers), CD44 (cellular stemness marker) and PD-L1 (tumor immune escape indicator) in the subcutaneous tumor tissues of nude mice. Compared with in the A549 group, the A549 + oe-TBX20 group exhibited significantly lower E-cadherin levels (Fig. 6B), whereas N-cadherin (Fig. 6C), vimentin (Fig. 6D), CD44 (Fig. 6E) and PD-L1 levels (Fig. 6F) were significantly greater (P<0.05). Conversely, compared with in the control group, the A549 + sh-TBX20 group demonstrated significantly higher E-cadherin levels, with significant reductions in N-cadherin, vimentin, CD44 and PD-L1 levels (P<0.05).

Effects of TBX20 overexpression and silencing on immune cell infiltration in subcutaneous tumors from nude mice. To assess the effects of TBX20 on immune cell infiltration in nude mice, flow cytometry was performed to detect the infiltration of $CD8^+$ T cells and $CD4^+$ T cells in subcutaneous tumor tissues, along with the proportions of M1 and M2 macrophages, and regulatory T cells (Tregs). The inoculation of human PBMCs into nude mice (lacking functional T cells) provides a reconstructed host environment capable of eliciting an immune response for human-derived tumors. $CD8^+$ T cells and $CD4^+$ T cells are the core components of PBMCs, whereas Tregs are also a functional subgroup present in PBMCs. Compared with in the A549 + sh-TBX20 group, the A549 + oe-TBX20 group exhibited significantly lower infiltration levels of $CD4^+$ T cells, $CD8^+$ T cells and M1 cells, but significantly greater infiltration levels of M2 cells and Tregs (P<0.05; Fig. 7). Conversely, compared with in the A549 + NC group, the A549 + sh-TBX20 group exhibited significantly higher infiltration levels of $CD4^+$ T cells, $CD8^+$ T cells, and M1 macrophages, but significantly lower infiltration levels of M2 macrophages and Tregs (P<0.05).

Discussion

TBX20 is a TF that serves a key regulatory role during development, although its expression patterns in tumor tissues remain poorly understood. As a member of the TBX1 subfamily, TBX1 acts as a tumor activator in prostate cancer by promoting ribosomal RNA gene transcription (7). In breast cancer, TBX1 expression levels are significantly higher in tumor tissues than in adjacent normal breast tissue, with gradual increases observed as tumor stages progress. Knocking down TBX1 expression can markedly inhibit the proliferation, colony formation, migration and invasion of breast cancer cell (19). TBX20 is classified as a member of the TBX1 subfamily, and shares homology with TBX1 in terms of protein structure (conserved T-box DNA-binding domain) and chromosomal distribution (20).

The present study investigated the biological functions of TBX20 in lung cancer cells, particularly its effects on cell viability, migration, invasion and spheroid formation. By establishing an A549 cell line overexpressing TBX20, it was revealed that TBX20 promoted malignant behaviors in lung cancer cells. Conversely, TBX20 knockdown significantly inhibited these malignant behaviors, indicating its crucial regulatory role in lung cancer progression. Previous studies have suggested that TBX20 is highly expressed in various tumors and is associated with poor prognosis (21,22). Consistent with these findings, in the present study, TBX20 was revealed to be highly expressed in lung cancer cell lines, and was able to regulate four key malignant phenotypes: Viability, migration, invasion and spheroid formation, with particularly enhanced spheroid formation capacity. This ability is a hallmark of

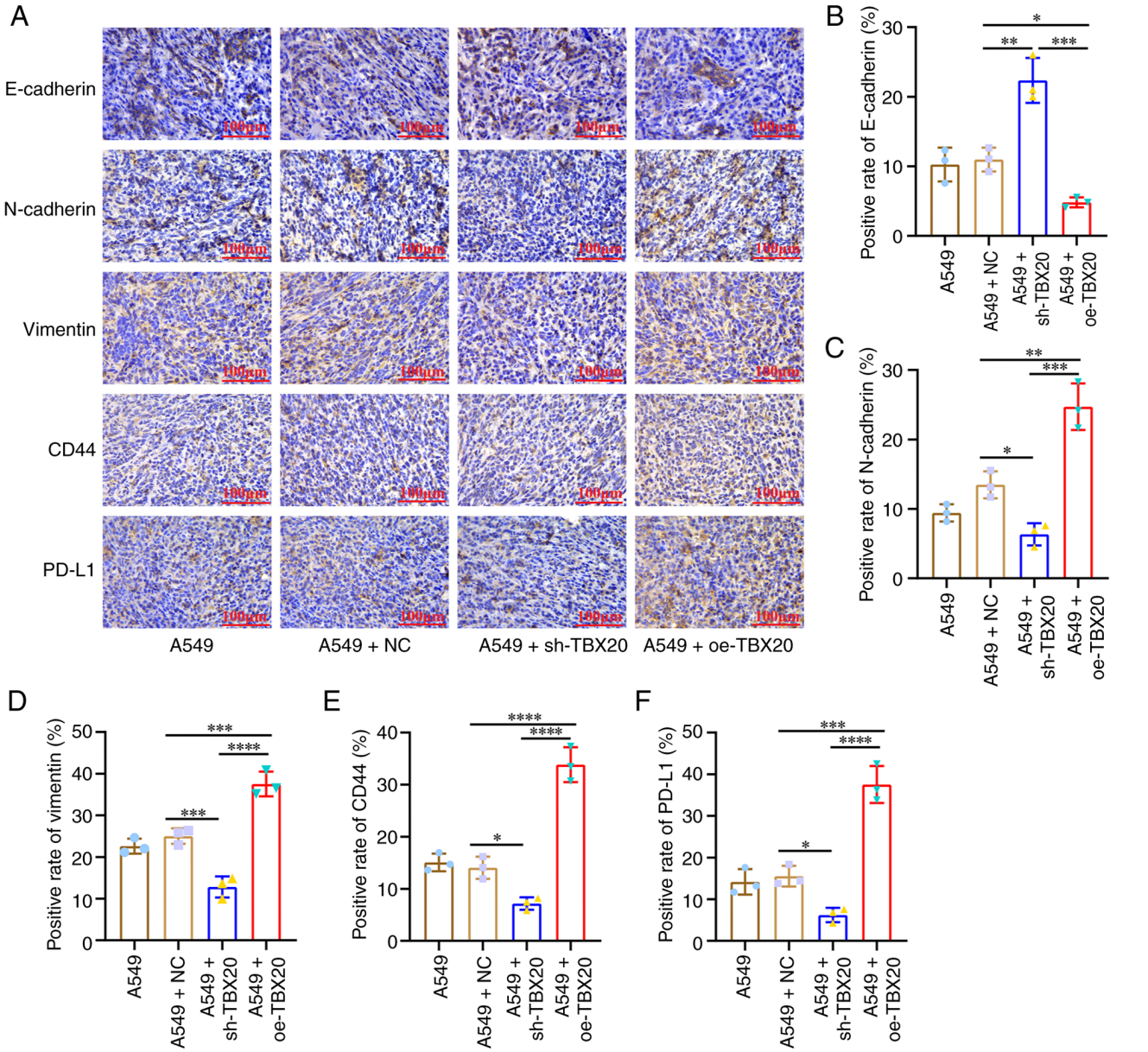

Figure 6. IHC staining of EMT and stemness indicators in subcutaneous tumor models of nude mice. (A) IHC staining of E-cadherin, N-cadherin, vimentin, CD44 and PD-L1 in A549 subcutaneous tumor models (magnification, x400). (B) E-cadherin, (C) N-cadherin, (D) vimentin, (E) CD44 and (F) PD-L1 positivity rates across different groups. Data are presented as the mean ± standard deviation (n=3). *P<0.05, **P<0.01, ***P<0.001 and ****P<0.0001. IHC, immunohistochemistry; NC, negative control; oe, overexpression; si, small interfering; TBX20, T-box transcription factor 20.

cancer stem cells (CSCs), which possess superior immune evasion capabilities (23). Furthermore, lung cancer cells with spheroid formation capacity typically exhibit enhanced resistance to chemotherapy and radiotherapy (24). Clinically, the spheroid formation capacity of lung cancer cells is a potential prognostic biomarker (25). Therefore, the development of immunotherapy strategies targeting TBX20-regulated tumor stem cells with spheroid formation and immune evasion capabilities could lead to novel breakthroughs for improving outcomes for patients with lung cancer.

To investigate the specific mechanisms of TBX20 in lung cancer cells the current study further examined markers associated with EMT, tumor stem cell characteristics and immune evasion. By comparing TBX20-overexpressing lung cancer cells with control cells, it was demonstrated that TBX20 overexpression significantly reduced E-cadherin expression, but increased N-cadherin, vimentin,CD44, Nanog, PD-L1, IL-6 and CCL2 expression. Similar phenomena were observed in the *in vivo* experiments. These findings indicated that TBX20 overexpression promotes malignant progression through EMT induction, enhanced stemness and immune evasion, thereby facilitating metastasis, therapy resistance and immune escape in lung cancer.

E-cadherin, an adhesion molecule in epithelial cells. Loss of E-cadherin weakens the adhesion force between cells, making cancer cells more likely to detach and spread to other parts. By contrast, N-cadherin, a mesenchymal cell adhesion molecule, is typically upregulated in lung cancer tissues; this elevated N-cadherin expression enhances cell adhesion and migration, thereby promoting tumor invasion

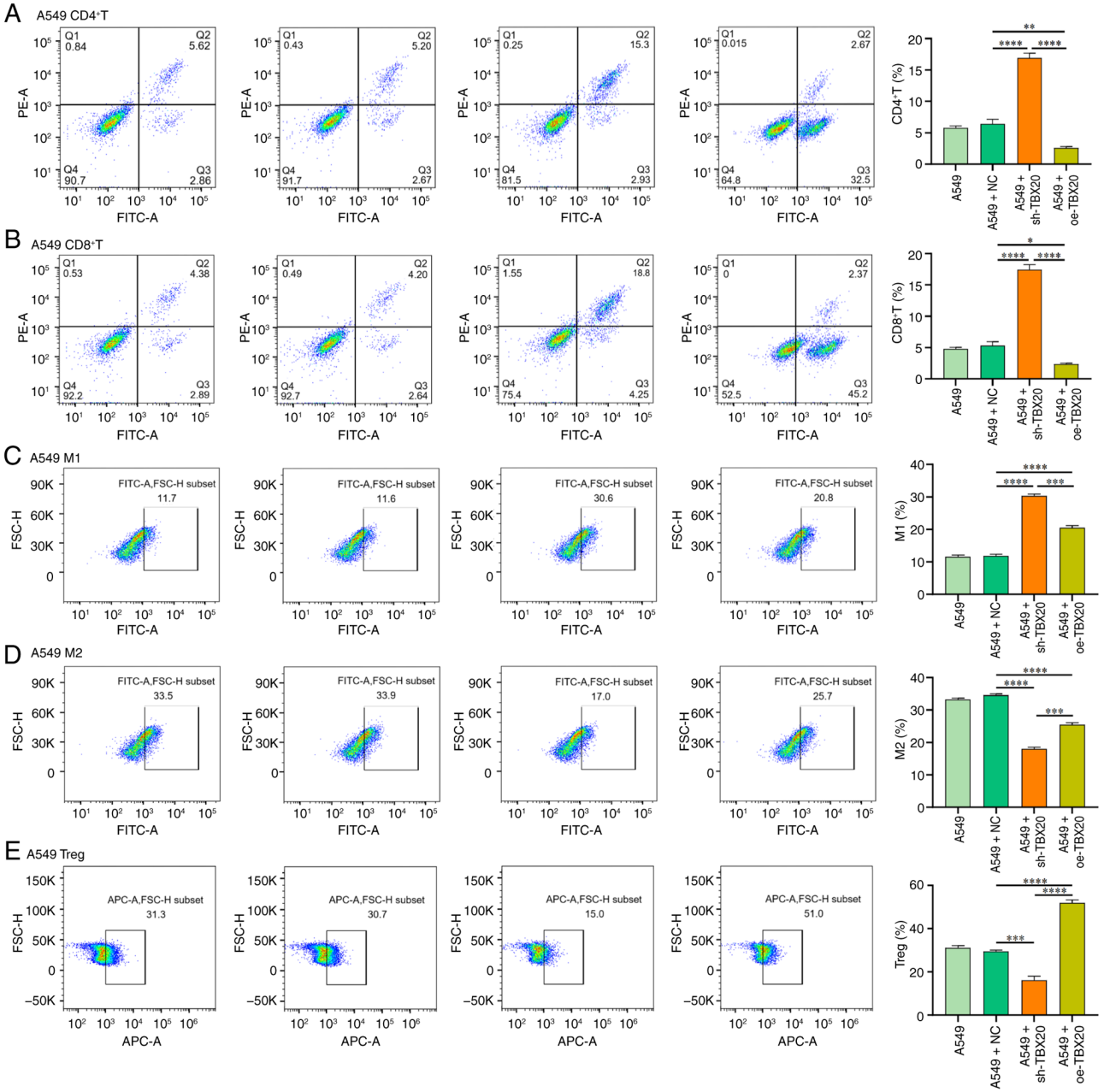

Figure 7. Flow cytometric analysis of CD4+ T cells, CD8+ T cells, M1 cells, M2 cells and Tregs. Infiltration levels of (A) CD4+ T cells, (B) CD8+ T cells, (C) M1 macrophages, (D) M2 macrophages and (E) Tregs in A549 cell xenograft tumors across different groups. Data are presented as the mean ± standard deviation (n=3). *P<0.05, **P<0.01, ***P<0.001 and ****P<0.0001. NC, negative control; oe, overexpression; si, small interfering; TBX20, T-box transcription factor 20; Treg, regulatory T cell.

and metastasis (26). Vimentin is an intermediate filament protein. During the EMT process, lung cancer cells increase the expression of Vimentin, acquiring the characteristics of mesenchymal cells, thereby enhancing their motility and invasiveness (27). In the current study, TBX20 overexpression led to decreased E-cadherin expression, and increased N-cadherin and vimentin expression, whereas TBX20 silencing resulted in elevated E-cadherin expression, and reduced N-cadherin and vimentin levels. These findings suggest that TBX20 silencing may suppress lung cancer cell invasion and metastasis by regulating the expression levels of EMT-associated proteins.

Both Sox2 and Nanog are stem cell TFs that have pivotal roles in maintaining the characteristics of tumor stem cells. In lung cancer, high expression levels of Sox2 and Nanog are closely associated with tumor invasiveness, chemotherapy resistance and EMT (28). CD44, a glycoprotein on the cell surface, is also highly expressed in lung cancer and is associated with the properties of tumor stem cells, promoting their self-renewal and chemotherapy resistance. Furthermore, CD44 contributes to the formation and remodeling of the tumor microenvironment (TME) by facilitating interactions between tumor cells and stromal cells, thereby creating favorable conditions for tumor growth and metastasis (29). The present study demonstrated that TBX20 overexpression increased the expression levels of Sox2, Nanog and CD44, whereas TBX20 silencing reduced these factors. These

findings suggest that TBX20 suppression may inhibit lung CSC characteristics by regulating the expression of the stem cell-associated factors Sox2 and Nanog, as well as the cell surface glycoprotein CD44, thereby affecting the invasiveness, chemotherapy resistance and metastatic capacity of lung cancer cells.

PD-L1 is typically upregulated on tumor cell surfaces (30). IL-6, a multifunctional cytokine, serves key roles in inflammatory responses, immune regulation and cell proliferation. IL-6 upregulates immune checkpoint molecules such as PD-L1, thereby enhancing tumor cell immune evasion capabilities (31). CCL2 (also known as monocyte chemotactic protein-1) is a key chemokine primarily secreted by tumor cells and tumor-associated stromal cells, which recruits immune cells such as monocytes, macrophages, myeloid-derived suppressor cells and Tregs into the TME, thereby promoting immune suppression and tumor progression (32). The present study demonstrated that TBX20 overexpression increased the expression levels of PD-L1, IL-6 and CCL2, whereas TBX20 knockdown reduced these factors. These findings suggest that inhibiting TBX20 may significantly modulate immune evasion mechanisms in lung cancer cells by regulating the expression of these immune factors.

In nude mouse tumor formation experiments, TBX20 overexpression significantly reduced the infiltration levels of $CD4^+$ T cells, $CD8^+$ T cells, and M1-type macrophages in subcutaneous tumor tissues, but increased the proportions of M2-type macrophages and Tregs. Conversely, when TBX20 was inhibited, these effects were reversed. These results indicate that TBX20 not only serves as a key factor driving the malignant behavior of tumor cells but also acts as a crucial regulator of the tumor immune microenvironment.

M1-type macrophages typically exert antitumor effects, whereas M2-type macrophages promote tumor growth, angiogenesis and tissue remodeling through multiple mechanisms, while suppressing adaptive immune responses (33). The present study demonstrated that knocking down TBX20 led to an increase in M1 and a decrease in M2. Compared to the TBX20 knockdown group, TBX20 overexpression significantly shifted the M1/M2 balance towards M2, which may be a critical factor in tumor progression. M2-type macrophages directly inhibit T-cell activation and proliferation by secreting immunosuppressive factors, such as IL-10 and TGF-β, and expressing immune checkpoint molecules such as PD-L1 (33). While Tregs serve a crucial role in maintaining immune tolerance, in the TME, they suppress antitumor immunity through multiple mechanisms. The present study demonstrated that the proportion of Tregs was significantly elevated in the TBX20-overexpressing group, which is consistent with the observed functional suppression of $CD4^+$ and $CD8^+$ T cells. Tregs competitively deplete IL-2 in the microenvironment, thereby inhibiting the effector functions of coexisting $CD8^+$ T cells, preventing these cells from effectively eliminating cancer cells (34). The enrichment of TBX20-induced Tregs may serve as a mechanism for tumor immune evasion. $CD8^+$ T cells, the core executors of antitumor immunity, exhibit reduced infiltration and functional suppression as hallmarks of immune evasion (35). In the present study, significantly decreased $CD8^+$ T-cell infiltration in the TBX20-overexpression group suggested that TBX20 created a microenvironment unfavorable for the survival and function of effector T cells.

The present study preliminarily demonstrated that TBX20 can induce EMT, enhance stemness and upregulate immune-related factors in A549 cells to promote immune evasion; however, its downstream signaling pathways remain unexplored and should be defined in future promoter deletion, DNA-binding mutagenesis and rescue experiments. Future research should focus on candidate pathways, such as BMP2/pSmad1/5/8 and PI3K/AKT/GSK3β/β-catenin to identify functionally dependent nodes. Furthermore, the animal sample size may have led to an underestimation of significant differences; therefore, the cohort will be expanded in subsequent experiments.

In conclusion, TBX20 was revealed to be highly expressed in lung cancer cells. The overexpression of TBX20 significantly increased lung cancer cell viability, migration, invasion and spheroid formation, whereas its knockdown reversed these effects. Mechanistic studies revealed that TBX20 may induce EMT, which is characterized by the downregulation of E-cadherin expression, and the upregulation of N-cadherin and vimentin expression. Additionally, TBX20 could enhance tumor cell stemness by increasing the expression of the stem cell marker CD44, and may promote immune evasion by upregulating immune-associated factors such as PD-L1. These findings highlight the pivotal regulatory role of TBX20 in the malignant phenotype of lung cancer cells, providing a potential therapeutic target for targeted therapy. Inhibiting TBX20 and its downstream factors could improve patient outcomes, reduce tumor recurrence and metastasis risks, and ultimately increase treatment efficacy and survival rates.

Acknowledgements

Not applicable.

Funding

No funding was received.

Availability of data and materials

The data generated in the present study may be requested from the corresponding author.

Authors' contributions

CX conceived and designed the study, analyzed data, conducted experiments and wrote and revised the manuscript. PZ, YZ and LL conducted experiments, performed analysis, and constructed figures. GW conducted experiments, established the methodology, analyzed data and revised the manuscript. All authors have read and approved the final manuscript.. CX and GW confirm the authenticity of all the raw data.

Ethics approval and consent to participate

The present study was approved by the Animal Ethics Committee of Fuzhou University Affiliated Provincial Hospital (approval no. IACUC-FPH-SL-20250527[1092]).

Patient consent for publication

Not applicable.

Competing interests

The authors declare that they have no competing interests.

References

1. Bray F, Laversanne M, Sung H, Ferlay J, Siegel RL, Soerjomataram I and Jemal A: Global cancer statistics 2022: GLOBOCAN estimates of incidence and mortality worldwide for 36 cancers in 185 countries. CA Cancer J Clin 74: 229-263, 2024.
2. Bi JH, Tuo JY, Xiao YX, Tang DD, Zhou XH, Jiang YF, Ji XW, Tan YT, Yuan HY and Xiang YB: Observed and relative survival trends of lung cancer: A systematic review of population-based cancer registration data. Thorac Cancer 15: 142-151, 2024.
3. Li D, Tian J and Zou Y: Advancing the understanding of the immune escape in lung cancer immunotherapy: Global trends, collaborations, and future directions. Hum Vaccin Immunother 22: 2628395, 2026.
4. Yi L, Zhou L, Shao B, Xiang T and Tang J: Multifaceted role of T-box transcription factor 4: From embryonic development to disease pathogenesis. Genes Dis 13: 101811, 2025.
5. Shimoda M, Sugiura T, Imajyo I, Ishii K, Chigita S, Seki K, Kobayashi Y and Shirasuna K: The T-box transcription factor Brachyury regulates epithelial-mesenchymal transition in association with cancer stem-like cells in adenoid cystic carcinoma cells. BMC Cancer 12: 377, 2012.
6. Dong L, Lyu X, Faleti OD and He ML: The special stemness functions of Tbx3 in stem cells and cancer development. Semin Cancer Biol 57: 105-110, 2019.
7. Wang N, Li Y, Wei J, Pu J, Liu R, Yang Q, Guan H, Shi B, Hou P and Ji M: TBX1 functions as a tumor suppressor in thyroid cancer through inhibiting the activities of the PI3K/AKT and MAPK/ERK pathways. Thyroid 29: 378-394, 2019.
8. Cui J, Zhang Y, Ren X, Jin L and Zhang H: TBX1 functions as a tumor activator in prostate cancer by promoting ribosome RNA gene transcription. Front Oncol 10: 616173, 2021.
9. Liu H, Song M, Sun X, Zhang X, Miao H and Wang Y: T-box transcription factor TBX1, targeted by microRNA-6727-5p, inhibits cell growth and enhances cisplatin chemosensitivity of cervical cancer cells through AKT and MAPK pathways. Bioengineered 12: 565-577, 2021.
10. Li S, Luo X, Sun M, Wang Y, Zhang Z, Jiang J, Hu D, Zhang J, Wu Z, Wang Y, *et al*: Context-dependent T-BOX transcription factor family: from biology to targeted therapy. Cell Commun Signal 22: 350, 2024.
11. Chakraborty S, Sengupta A and Yutzey KE: Tbx20 promotes cardiomyocyte proliferation and persistence of fetal characteristics in adult mouse hearts. J Mol Cell Cardiol 62: 203-213, 2013.
12. Luo J, Chen JW, Zhou J, Han K, Li S, Duan JL, Cao CH, Lin JL, Xie D and Wang FW: TBX20 inhibits colorectal cancer tumorigenesis by impairing NHEJ-mediated DNA repair. Cancer Sci 113: 2008-2021, 2022.
13. Tang Y, Aryal S, Geng X, Zhou X, Fast VG, Zhang J, Lu R and Zhou Y: TBX20 improves contractility and mitochondrial function during direct human cardiac reprogramming. Circulation 146: 1518-1536, 2022.
14. Zhang D, Shang X, Ji Q and Niu L: Exploring genetic mapping and co-expression patterns to illuminate significance of Tbx20 in cardiac biology. Transgenic Res 34: 5, 2025.
15. Livak KJ and Schmittgen TD: Analysis of relative gene expression data using real-time quantitative PCR and the 2(-Delta Delta C(T)) Method. Methods 25: 402-408, 2001.
16. Emile MH, Emile SH, El-Karef AA, Ebrahim MA, Mohammed IE and Ibrahim DA: Association between the expression of epithelial-mesenchymal transition (EMT)-related markers and oncologic outcomes of colorectal cancer. Updates Surg 76: 2181-2191, 2024.
17. Zhou J, Wang H, Che J, Xu L, Yang W, Li Y and Zhou W: Silencing of microRNA-135b inhibits invasion, migration, and stemness of CD24+CD44+ pancreatic cancer stem cells through JADE-1-dependent AKT/mTOR pathway. Cancer Cell Int 20: 134, 2020.
18. Jin SX, Liu BN, Ji HJ, Wu JR, Li BL, Gao XL, Li N, Zheng ZD and Du C: Serum cytokines and creatinine/cystatin C ratio as prognostic biomarkers in advanced cancer patients treated with anti-PD-1/PD-L1 therapy. Support Care Cancer 32: 370, 2024.
19. Huang S, Shu X, Ping J, Wu J, Wang J, Shidal C, Guo X, Bauer JA, Long J, Shu XO, *et al*: TBX1 functions as a putative oncogene of breast cancer through promoting cell cycle progression. Carcinogenesis 43: 12-20, 2022.
20. Takatori N, Hotta K, Mochizuki Y, Satoh G, Mitani Y, Satoh N, Satou Y and Takahashi H: T-box genes in the ascidian Ciona intestinalis: Characterization of cDNAs and spatial expression. Dev Dyn 230: 743-753, 2004.
21. Li J, Huan J, Yang F, Chen H, Wang M and Heng X: Identification and validation of a seizure-free-related gene signature for predicting poor prognosis in lower-grade gliomas. Int J Gen Med 14: 7399-7410, 2021.
22. Zhang L, Li D, Du F, Huang H, Yuan C, Fu J, Sun S, Tian T, Liu X, Sun H, *et al*: A panel of differentially methylated regions enable prognosis prediction for colorectal cancer. Genomics 113: 3285-3293, 2021.
23. Terry S, Savagner P, Ortiz-Cuaran S, Mahjoubi L, Saintigny P, Thiery JP and Chouaib S: New insights into the role of EMT in tumor immune escape. Mol Oncol 11: 824-846, 2017.
24. Zhao W, Luo Y, Li B and Zhang T: Tumorigenic lung tumorospheres exhibit stem-like features with significantly increased expression of CD133 and ABCG2. Mol Med Rep 14: 2598-2606, 2016.
25. Herreros-Pomares A, de-Maya-Girones JD, Calabuig-Fariñas S, Lucas R, Martínez A, Pardo-Sánchez JM, Alonso S, Blasco A, Guijarro R, Martorell M, *et al*: Lung tumorspheres reveal cancer stem cell-like properties and a score with prognostic impact in resected non-small-cell lung cancer. Cell Death Dis 10: 660, 2019.
26. Loh CY, Chai JY, Tang TF, Wong WF, Sethi G, Shanmugam MK, Chong PP and Looi CY: The E-Cadherin and N-Cadherin switch in epithelial-to-mesenchymal transition: Signaling, therapeutic implications, and challenges. Cells 8: 1118, 2019.
27. Berr AL, Wiese K, Dos Santos G, Koch CM, Anekalla KR, Kidd M, Davis JM, Cheng Y, Hu YS and Ridge KM: Vimentin is required for tumor progression and metastasis in a mouse model of non-small cell lung cancer. Oncogene 42: 2074-2087, 2023.
28. Chu X, Tian W, Ning J, Xiao G, Zhou Y, Wang Z, Zhai Z, Tanzhu G, Yang J and Zhou R: Cancer stem cells: advances in knowledge and implications for cancer therapy. Signal Transduct Target Ther 9: 170, 2024.
29. Alaei E, Farahani N, Orouei S, Alimohammadi M, Daneshi S, Mousavi T, Mahmoodieh B, Taheriazam A, Rahimzadeh P and Hashemi M: The clinicopathologic and prognostic value of CD44 expression in patients with non-small cell lung cancer: A systematic review and meta-analysis. Mol Cell Probes 81: 102028, 2025.
30. Li Z, Wang T, Liu J, Qi W, Lv Q, Xu Y and Tian L: The mechanism and research progress of PD-1/PD-L1 on immune escape of lung cancer. Transl Cancer Res 14: 6041-6051, 2025.
31. Jing B, Wang T, Sun B, Xu J, Xu D, Liao Y, Song H, Guo W, Li K, Hu M, *et al*: IL6/STAT3 signaling orchestrates premetastatic niche formation and immunosuppressive traits in lung. Cancer Res 80: 784-797, 2020.
32. Kohli K, Pillarisetty VG and Kim TS: Key chemokines direct migration of immune cells in solid tumors. Cancer Gene Ther 29: 10-21, 2022.
33. Hao D and Chen S: Targeting tumor-associated macrophages in non-small cell lung cancer: Mechanisms, prognosis, and therapeutic opportunities. Front Immunol 16: 1679537, 2025.
34. Li X, Pan L, Li W, Liu B, Xiao C, Chew V, Zhang X, Long W, Ginhoux F, Loscalzo J, *et al*: Deciphering immune predictors of immunotherapy response: A multiomics approach at the pan-cancer level. Cell Rep Med 6: 101992, 2025.
35. Yan D, Wang Y, Zhang L, Li Y, Gong Y, Liu H, Ma X and Pang J: ARTN drives CD8+ T cell exhaustion via the GFRα3-RET-PI3K/AKT Axis to promote TNBC progression. Cell Signal 141: 112397, 2026.